Generation of intensity difference squeezed state at a wavelength of 1.34 μm

Meiru Huo (霍美如)[1], Jiliang Qin (秦际良)[1], Yingrong Sun (孙颖榕)[1], Zhihui Yan (闫智辉)[1,2], and Xiaojun Jia (贾晓军)[1,2,*]

[1]*State Key Laboratory of Quantum Optics and Quantum Optics Devices, Institute of Opto-Electronics, Shanxi University, Taiyuan 030006, China*

[2]*Collaborative Innovation Center of Extreme Optics, Shanxi University, Taiyuan 030006, China*

Corresponding author: jiaxj@sxu.edu.cn

Received February 5, 2018; accepted April 3, 2018; posted online May 4, 2018

The intensity difference squeezed state, which means that the fluctuation of the intensity difference between signal and idler beams is less than that of the corresponding shot noise level (SNL), plays an important role in high sensitivity measurement, quantum imaging, and quantum random numbers generation. When an optical parametric oscillator consisting of a type-II phase-matching periodically poled KTiOPO$_4$ crystal operates above the threshold, an intensity difference squeezed state at a telecommunication wavelength can be obtained. The squeezing of 7.7 ± 0.5 dB below the SNL is achieved in an analysis frequency region of 2.4–5.0 MHz.

OCIS codes: 270.0270, 270.6570.

doi: 10.3788/COL201816.052701.

With development of various quantum optics researches, non-classical states of light with diverse quantum properties have been widely used in all kinds of related theoretical and experimental researches[1]. As is known to all, a single-mode squeezed state of light[2,3], whose quantum noise is one quadrature lower than the standard shot noise level (SNL), has been used in quantum key distribution and precision measurements[4–9]. If correlation variances of both quadratures of a two-mode state are below the corresponding SNL, this state is defined as a two-mode squeezed state of light, i.e., the Einstein–Podolsky–Rosen (EPR) entangled state of light[10]. Because of this special correlation characteristic, the EPR entangled state has been widely utilized in quantum teleportation, quantum entanglement swapping, quantum computing, quantum metrology, and so on[11–14]. On the other hand, there is another kind of non-classical state of light with a correlation variance of only an intensity difference below the corresponding SNL, which is usually called the intensity difference squeezed state. There are two main methods to generate an intensity difference squeezed state of light. One method is based on four-wave mixing (FWM) in atomic ensembles[15–25], where the relative intensity difference of the probe and conjugate beams is squeezed compared with the corresponding SNL. Up till now, the intensity difference squeezed state at the D1 and D2 lines of ^{85}Rb and ^{87}Rb generated by the method of FWM in atomic ensembles reaches 9.2 dB below the SNL[15]. The advantage of this method is that the frequency of the generated intensity difference squeezed state is suitable for the interaction with the atomic assemble. The other method of producing the intensity difference squeezed state is using the optical parametric process[26–31], where the correlation variance of the simultaneously generated signal and idler beams from an optical parametric

oscillator (OPO) operating above the threshold can be compressed to the noise level far below the corresponding SNL. In 1998, the noise of the intensity difference between the twin beams at wavelengths of 1039 and 1090 nm reached 9.2 dB below the SNL[27].

Moreover, the intensity of generated twin beams is usually in the ten milliwatts order[32], which is much higher than those of the single-mode squeezed state and the two-mode EPR entangled state, and thus, the intensity difference squeezed state is widely applied in the measurement for modulation absorption of the sub-shot-noise limit, recovery of a weak signal, and measurement for weak absorption[32–36]. In 1999, a measurement of the intensity difference squeezed state satisfying all the quantum non-demolition criteria is experimentally achieved[33]. Another advantage of its application is its simplicity detection system, e.g., the correlation variance of the intensity difference squeezed state can be directly measured without the help of a local oscillator[26]. Thus, it has been widely used in several quantum technologies, such as quantum imaging and true quantum random numbers generation[37–41]. With the development of quantum network technology, long-distance quantum measurement and a quantum image are required. Because an optical fiber is an effective transfer medium, the generation of the non-classical state at the transmission window of the optical fiber is an important demand for extending its application[42]. In this Letter, a robust intensity difference squeezed state at a telecommunication wavelength of 1.3 μm has been generated by a compact optical device, which is integrated on an invar steel base with a total volume of about 50 mm × 140 mm × 80 mm and good stability. A broadband intensity difference squeezed state of light is experimentally generated by an OPO operating above the threshold with a type-II periodically poled

KTiOPO$_4$ (PPKTP) crystal, and the squeezing of 7.7 dB is realized in the analysis frequency region of 2.4–5.0 MHz.

Figure 1 shows optical parametric conversion in an OPO, which usually satisfies quasi-phase-matching (QPM) conditions[43],

$$\omega_0 = \omega_1 + \omega_2,$$
$$k_0 = k_1 + k_2 + mK_g, \tag{1}$$

where the subscripts 0, 1, 2 are corresponding to pump, signal, and idler beams, respectively. $\omega_j \, (j = 0, 1, 2)$ and k_j are their angular frequency and wave vector in the propagational direction, respectively. K_g is a periodically poled vector, and m is the QPM order with integer values. Equation (1) describes the energy and momentum conservations during the optical parametric conversation in the OPO. For the intensity difference squeezed state generating process, conservations for energy and momentum become

$$k_0^y = k_1^z + k_2^y + mK_g^{\mathrm{II}}, \tag{2}$$

where y, z denote the y, z axes of the PPKTP crystal, K_g^{II} is for type-II QPM, and $m = 1$ (34). Equation (2) describes a process that a horizontal (corresponding to the y axis of the crystal) polarization pump laser can convert to a vertical (corresponding to the z axis of the crystal) polarization signal, and horizontal polarization idler beams with near-degenerate optical frequencies when the appropriate crystal temperature of PPKTP and perfect beam-matching between the pump and the OPO are obtained. When the pump power of the OPO is above its threshold, the noise spectrum for the intensity difference of the output beams from the OPO is calculated as[31,39,44]

$$S_{\mathrm{IDS}}(\Omega) = S_{\mathrm{SNL}}\left(1 - \frac{\eta\xi}{1 + \Omega^2\tau_C^2}\right), \tag{3}$$

where S_{SNL} is the corresponding SNL. Ω is the analysis frequency of measurement, η is the total quantum detection efficiency, and τ_C is the storage time of the cavity, which is determined by the linewidth of the OPO. $\xi = T/(T + \delta)$ is the escape efficiency of the OPO, T is the transmission efficiency of the output mirror of the OPO for the infrared beam, and δ is the optical loss of the cavity. The actual values in our experimental system for these parameters are $\Omega = 2.4$–5.0 MHz, $\eta = 0.95$, $\xi = 95.1\%$, and $\tau_C = 0.0085$ μs. Substituting these parameter values into Eq. (3), the calculated result of the intensity difference squeezed state noise is obtained with S_{SNL} normalized to a unitary one, which is about 9 dB below the corresponding SNL in the frequency range of 2.4–5.0 MHz.

Figure 2 exhibits the experimental schematic for the generation of the intensity difference squeezed state at a telecommunication wavelength. A Nd:YVO$_4$/LiB$_3$O$_5$ (LBO) laser with a dual wavelength of 671 and 1342 nm (Yuguang Company) is used as the optical source, which outputs powers of 2.8 W at 671 nm and
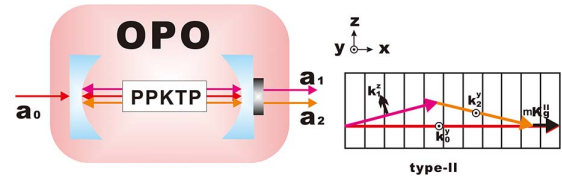

Fig. 1 Optical parametric conversation and QPM process of the pump, signal, and idler beams in the OPO. $a_j \, (j = 0, 1, 2)$ and k_j denote optical modes and wave vectors of the pump, signal, and idler, respectively. Superscripts y and z are corresponding to the y and z axes of the PPKTP crystal. K_g^{II} is the periodically poled vector for type-II QPM, and m is the QPM order with integer values.
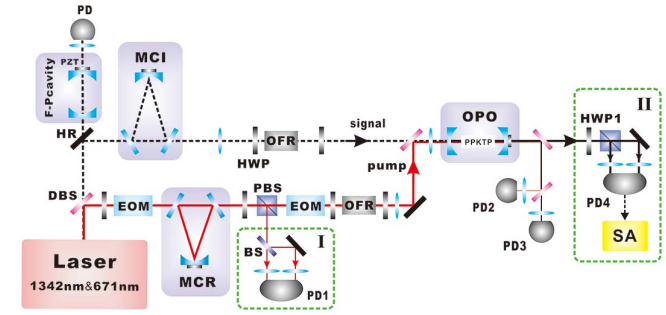

Fig. 2 Experimental schematic of generating the intensity difference squeezed state. Laser, Nd:YVO4/LBO; DBS, dichroic beam splitter; HR, mirror with reflectivity higher than 99.95%; EOM, electro-optical modulator; MCR (MCI), mode-cleaner for red beam (infrared beam); OFR, optical Faraday rotator; HWP, half-wave plate; PBS, polarization beam splitter; BS, 50:50 beam splitter; OPO, optical parametric oscillator; PD, photoelectric detector; PZT, piezoelectric ceramic; SA, spectrum analyzer.

850 mW at 1342 nm, respectively. Its single-frequency operation condition is monitored by a Fabry–Perot (F-P) cavity. The two wavelength lasers are separated by a dichroic beam splitter (DBS), and each of them passes through a mode-cleaner for a red beam and an infrared beam (MCR and MCI), respectively, for spatial–temporal mode-filtering and the intensity stabilizing of the beams. The finesses of the MCR and MCI are 400 at 671 nm and 300 at 1342 nm mode-cleaners, respectively. The OPO cavity is in a standing wave cavity configuration with a pair of concave mirrors as the input and output mirrors, whose diameter is 10 mm and the curvature radius is 50 mm. The 1 mm × 2 mm × 12 mm PPKTP crystal is placed in the middle of the OPO. The temperature of the crystal is carefully controlled by a copper oven driven by a thermoelectric cooler for realizing the perfect phase-matching of the crystal. The distance between two mirrors of the OPO is selected as 104 mm, and, thus, the waist of 46 μm for the 1342 nm infrared mode is obtained in the center of the crystal. The films coated on the input mirror have reflectivity $R > 99.8\%$ at 1342 nm, and transmission $T = 20\%$ at 671 nm; on the output mirror have $T = 13\%$ at 1342 nm, and $R > 99.9\%$ at 671 nm. In this condition, the pump mode can oscillate in the OPO. When the OPO

is pumped above the threshold, the signal and idler modes matching the energy and momentum conservations with minimal loss can oscillate first in the OPO cavity through mode competition and form a stable output beam of the OPO. Thus, the pump mode, signal mode, and idler mode can be simultaneously resonant in the OPO. The threshold of the OPO for pump power is 103 mW. In the beginning, an infrared beam (signal beam) is injected into the OPO to calibrate the mode-matching of the OPO cavity and the detection path for the infrared beam. It is blocked when the intensity difference squeezing is obtained and measured. The red beam is modulated by an electro-optic modulator (EOM), which generates an error signal for locking the length of the OPO to resonate with the red beam via the Pound–Drever–Hall sideband frequency stabilization technique. Photo-electronic detectors (PD2, PD3) are applied to measure the optical modes of the infrared and the red, and PD2 is also used to help lock the length of the OPO[45]. In the end, when a horizontal polarization pump laser with power of 120 mW is injected into the OPO, a stable intensity difference squeezed state with power of 6 mW is generated[26].

An all-solid-state laser source usually has a high noise in the low frequency region, which results from the resonant relaxation oscillation[46,47]. The extra noise in the pump laser will participate in the parametric conversion in the OPO and, thus, inevitably decrease quantum correlations of the twin beams[47]. The noise of the red laser out of the MCR is first measured by a detection system consisting of a 50:50 beam splitter (BS) and a two-diode PD1, as shown in Fig. 2. The red curve is measured when two photodiodes of the detector are injected with the light of the two outputs of the BS, and the blue curve is measured when the light injected into one photodiode is blocked. As shown in Fig. 3, the red curve is 3 dB higher than the blue after an analysis frequency of 2.4 MHz, which indicates that the noise level of the red laser achieves SNL after a frequency of 2.4 MHz, owing to good linearity of the detector[48].
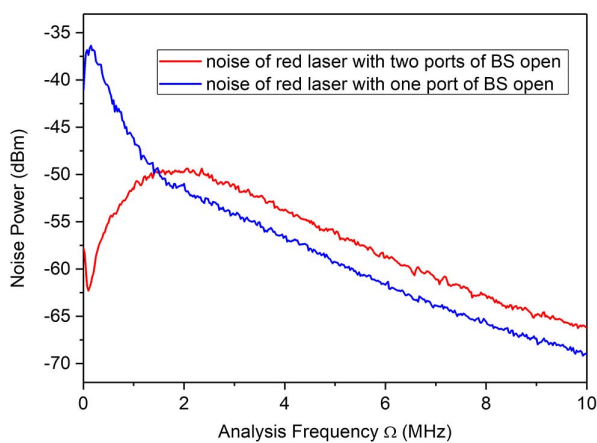

Fig. 3 Measurement for noise of the red laser. The red curve is measured when two photodiodes of the homodyne detector (PD1) are injected with a red laser, and the blue curve is measured by blocking one photodiode of PD1.
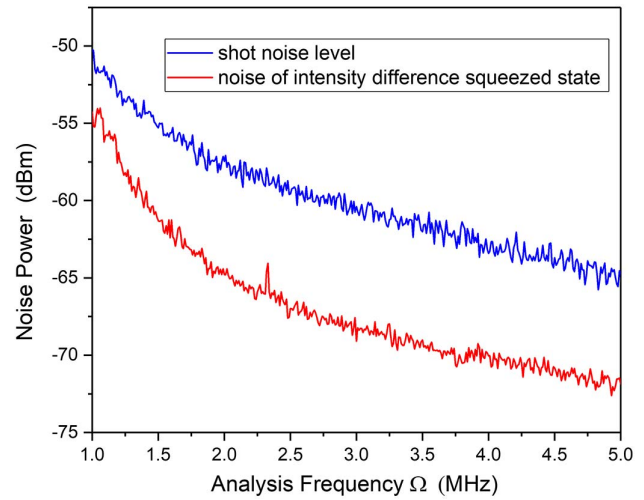

Fig. 4 Noise power of the generated intensity difference squeezed state versus different analysis frequencies. The blue curve is the SNL, and the red curve is the noise of the intensity difference squeezed state.

In the frequency region lower than 2.4 MHz, resonant relaxation oscillation of the laser leads to a high noise level, as the blue curve shows. The resolution bandwidth (RBW) and video bandwidth (VBW) of the spectrum analyzer (SA) are set at 100 kHz and 100 Hz, respectively.

Figure 4 shows the measured noise power of the generated intensity difference squeezed state. The precise measurement of the correlation noise and its corresponding SNL is important in the experiment. The noise power of the output twin beams from the OPO is recorded by an SA (EB4411, Agilent) connected with alternating current of PD4, which is a homemade two-photodiode detector, and an intensity difference squeezed state of 7.7 ± 0.5 dB below SNL is obtained in the frequency region of 2.4 and 5.0 MHz. RBW and VBW parameters are set at 30 kHz and 100 Hz, respectively. The corresponding SNL is obtained by adjusting the half-wave plate (HWP1) with 22.5° (the angle between the axes of the plate and the polarizer), and the combination of the HWP and the polarizing beam splitter (PBS) acts as the usual 50:50 BS. Thus, the signal beam and idler beam are, respectively, divided into two parts with the same power. Because the frequencies of the signal beam and idler beam are not the same, they cannot interfere in each path after the polarizer. Although extra noise lies in both the signal beam and idler beam, the noise can be subtracted because one half and the other half of the signal (idler) beam are separately incident to the two photodiodes in PD4. In this condition, the difference of the photocurrent recorded by the SA gives the SNL for the intensity of a beam the same as the generated twin beams. As shown in Refs. [26,27,30,32,49], the measured SNL almost equals the noise of the coherent state with the same power as the generated signal and idler beams. When HWP1 is rotated by 0°, the wave plate does not play any role in the output beams, and the noise power of the intensity difference squeezed state is consequently detected by PD4[26].

In summary, an intensity difference squeezed state of 7.7 ± 0.5 dB below the corresponding SNL in the frequency region of 2.4–5.0 MHz is generated by an OPO operating above threshold with a type-II PPKTP crystal. Pump laser noise is filtered by MCR to help produce a good intensity difference squeezed state. Since high squeezing is always useful for quantum communication protocols, further improving the degree of squeezing is meaningful. If the extra loss in the OPO is better restrained, the squeezing will be obviously improved. For example, the extra loss in the OPO of our current system is 0.67%, so if it can be reduced to 0.3%, the estimated squeezing can be enhanced to about 11 dB in principle. The OPO with a compact and stable configuration provides convenience and versatility for generating quantum correlated twin beams. Moreover, the generated intensity difference squeezed state at 1.34 µm as a two-color quantum correlated twin beam can greatly contribute to generating multi-color quantum correlated beams, which can connect systems of different natures in future quantum information networks, and is promising in applications of long-distance optical fiber channels quantum communication[50].

References

1. S. L. Braunstein and P. van Loock, Rev. Mod. Phys. **77**, 513 (2005).
2. C. Zhou, C. Zhang, H. Liu, K. Liu, H. Sun, and J. Gao, Chin. Opt. Lett. **15**, 092703 (2017).
3. N. Huo, C. Zhou, H. Sun, K. Liu, and J. Gao, Chin. Opt. Lett. **14**, 062702 (2016).
4. N. J. Cerf, M. Levy, and G. V. Assche, Phys. Rev. A **63**, 052311 (2001).
5. R. G. Patron and N. J. Cerf, Phys. Rev. Lett. **102**, 130501 (2009).
6. The LIGO Scientific Collaboration, Nat. Photon. **7**, 613 (2013).
7. N. Treps, N. Grosse, W. P. Bowen, C. Fabre, H. A. Bachor, and P. K. Lam, Science **301**, 940 (2003).
8. H. Yonezawa, D. Nakane, T. A. Wheatley, K. Iwasawa, S. Takeda, H. Arao, K. Ohki, K. Tsumura, D. W. Berry, T. C. Ralph, H. M. Wiseman, E. H. Huntington, and A. Furusawa, Science **337**, 1514 (2012).
9. A. A. Berni, T. Gehring, B. M. Nielsen, V. Handchen, M. G. A. Paris, and U. L. Anderson, Nat. Photon. **9**, 577 (2015).
10. Z. Y. Ou, S. F. Pereira, H. J. Kimble, and K. C. Peng, Phys. Rev. Lett. **68**, 3663 (1992).
11. A. Furusawa, J. L. Sorensen, S. L. Braunstein, C. A. Fuchs, H. J. Kimble, and E. S. Polzik, Science **282**, 706 (1998).
12. X. J. Jia, X. L. Su, Q. Pan, J. R. Gao, C. D. Xie, and K. C. Peng, Phys. Rev. Lett. **93**, 250503 (2004).
13. X. L. Su, S. H. Hao, X. W. Deng, L. Y. Ma, M. H. Wang, X. J. Jia, C. D. Xie, and K. C. Peng, Nat. Commun. **4**, 2828 (2013).
14. V. Giovannetti, S. Lloyd, and L. Maccone, Nat. Photon. **5**, 222 (2011).
15. R. C. Pooser, A. M. Marino, V. Boyer, K. M. Jones, and P. D. Lett, Opt. Express **17**, 16722 (2009).
16. R. E. Slusher, L. W. Hollberg, B. Yurke, J. C. Mertz, and J. F. Valley, Phys. Rev. Lett. **55**, 2409 (1985).
17. C. F. McCormick, A. M. Marino, V. Boyer, and P. D. Lett, Phys. Rev. A **78**, 043816 (2008).
18. C. F. McCormick, V. Boyer, E. Arimondo, and P. D. Lett, Opt. Lett. **32**, 178 (2007).
19. R. Ma, W. Liu, Z. Z. Qin, X. J. Jia, and J. R. Gao, Phys. Rev. A **96**, 043843 (2017).
20. Z. Z. Qin, L. M. Cao, H. L. Wang, A. M. Marino, W. P. Zhang, and J. T. Jing, Phys. Rev. Lett. **113**, 023602 (2014).
21. L. M. Cao, J. Qi, J. J. Du, and J. T. Jing, Phys. Rev. A **95**, 023803 (2017).
22. L. M. Cao, J. J. Du, J. L. Feng, Z. Z. Qin, A. M. Marino, M. I. Kolobov, and J. T. Jing, Opt. Lett. **42**, 1201 (2017).
23. H. L. Wang, C. Fabre, and J. T. Jing, Phys. Rev. A **95**, 051802 (2017).
24. J. J. Du, L. M. Cao, K. Zhang, and J. T. Jing, Appl. Phys. Lett. **110**, 241103 (2017).
25. W. Wang, L. M. Cao, Y. B. Lou, J. J. Du, and J. T. Jing, Appl. Phys. Lett. **112**, 034101 (2018).
26. A. Heidmann, R. J. Horowicz, S. Reynaud, E. Giacobino, C. Fabre, and G. Camy, Phys. Rev. Lett. **59**, 2555 (1987).
27. J. R. Gao, F. Y. Cui, C. Y. Xue, C. D. Xie, and K. C. Peng, Opt. Lett. **23**, 870 (1998).
28. J. Laurat, T. Coudreau, N. Treps, A. Maître, and C. Fabre, Phys. Rev. Lett. **91**, 213601 (2003).
29. Y. Zhang, K. Kasai, and M. Watanabe, Opt. Express **11**, 14 (2003).
30. R. X. Guo, X. J. Jia, C. D. Xie, and K. C. Peng, Opt. Commun. **211**, 243 (2002).
31. X. L. Su, A. H. Tan, X. J. Jia, Q. Pan, C. D. Xie, and K. C. Peng, Opt. Lett. **31**, 1133 (2006).
32. P. H. S. Ribeiro, C. Schwob, A. Maître, and C. Fabre, Opt. Lett. **22**, 1893 (1997).
33. H. Wang, Y. Zhang, Q. Pan, H. Su, A. Porzio, C. D. Xie, and K. C. Peng, Phys. Rev. Lett. **82**, 1414 (1999).
34. L. Yang and Y. Xia, Chin. Opt. Lett. **15**, 052701 (2017).
35. C. D. Nabors and R. M. Shelby, Phys. Rev. A **42**, 556 (1990).
36. T. A. B. Kennedy, Phys. Rev. A **44**, 2113 (1991).
37. G. Brida, M. Genovese, and I. Ruo-Berchera, Nat. Photon. **4**, 227 (2010).
38. T. Lunghi, J. B. Brask, C. C. W. Lim, Q. Lavigne, J. Bowles, A. Martin, H. Zbinden, and N. Brunner, Phys. Rev. Lett. **114**, 150501 (2015).
39. Q. Zhang, X. W. Deng, C. X. Tian, and X. L. Su, Opt. Lett. **42**, 895 (2017).
40. J. Brendel, N. Gisin, W. Tittel, and H. Zbinden, Phys. Rev. Lett. **82**, 2594 (1999).
41. Y. C. Zhu, J. H. Shi, H. Li, and G. H. Zeng, Chin. Opt. Lett. **12**, 071101 (2014).
42. Y. H. Zheng, Z. Q. Wu, M. R. Huo, and H. J. Zhou, Chin. Phys. B **22**, 094206 (2013).
43. M. R. Huo, J. L. Qin, Z. H. Yan, X. J. Jia, and K. C. Peng, Appl. Phys. Lett. **109**, 221101 (2016).
44. C. Fabre, E. Giacobino, A. Heidmann, and S. Reynaud, J. Phys. **50**, 1209 (1989).
45. J. L. Qin, Z. H. Yan, M. R. Huo, X. J. Jia, and K. C. Peng, Chin. Opt. Lett. **14**, 122701 (2016).
46. H. D. Lu, Y. R. Guo, and K. C. Peng, Opt. Lett. **40**, 5196 (2015).
47. Y. Wang, H. Shen, X. L. Jin, X. L. Su, C. D. Xie, and K. C. Peng, Opt. Express **18**, 6149 (2010).
48. H. P. Yuen and V. W. S. Chan, Opt. Lett. **8**, 177 (1983).
49. J. Mertz, T. Debuisschert, A. Heidmann, C. Fabre, and E. Giacobino, Opt. Lett. **16**, 1234 (1991).
50. M. A. Shemis, A. M. Ragheb, E. Alkhazraji, M. A. Esmail, H. Fathallah, S. Alshebeili, and M. Z. M. Khan, Chin. Opt. Lett. **15**, 100604 (2017).